Supplementary Information: The interplay of stiffness and force anisotropies drive embryo elongation

Thanh TK Vuong-Brender, Martine Ben Amar, Julien Pontabry and Michel Labouesse

Contents

1 Supplementary SI1: An overview of the early phase of *C. elegans* embryonic elongation 2

2 Supplementary SI2: The *C. elegans* embryonic epidermis is under biaxial stress loading along the AP and DV directions 2

3 Supplementary SI3: Comparison of two methods to analyze laser ablation responses using the recoil dynamics and the cut opening at equilibrium 4

4 Supplementary SI4: The ratio of the minor to major axis of the cut opening at equilibrium does not depend on the cut length 6

5 Supplementary SI5: Modeling of the *C. elegans* embryo as a capped thin-wall pressured vessel and calculation of the anisotropy of stress 6
5.1 Anisotropy of stress for an axisymmetric thin-wall pressured vessel 6
5.2 Anisotropy of stress for the body seam cell V3 of *C. elegans* embryo 9

6 Supplementary SI6: The Hooke's law written for seam and DV epidermal cells 11
6.1 Supplementary SI6A: The Hooke's law written for seam cells 11
6.2 Supplementary SI6B: The Hooke's law written for DV epidermal cells 11

7 Supplementary SI7: Cracks opening in orthotropic and fiber-reinforced planes 12
7.1 Introduction 12
7.2 Fracture in orthotropic linear elasticity 12
7.3 Definition of two complex functions 13
7.4 Fiber model in finite elasticity 14
7.5 Fiber versus orthotropic elasticity in extension 15
7.6 Fiber versus orthotropic elasticity in the case of shear deformation 15
7.7 How to evaluate the residual stress from the crack opening 16

8 Supplementary SI8: Modeling the DV epidermis as an orthotropic material 16

9 Supplementary SI9: Calculation of the ratio of Young moduli between the seam cell H1 and the head HYP7 cell matrix 17

10 Supplementary SI10: Calculation of K and DV/AP Young moduli ratio for a fiber-reinforced material 18

1 Supplementary SI1: An overview of the early phase of *C. elegans* embryonic elongation

Soon after the ventral enclosure has completed, *C. elegans* embryos elongate from a lima-bean shape to the characteristic cylindrical shape, resulting in a 4-fold increase in length and approximately a 2-fold decrease in diameter[1] (figure 1a). The elongation is thought to be driven by cell shape changes, as can be most easily observed among seam cells (figure 1a). Muscle contractions, starting about midway through the process, are essential, since muscle-defective embryos are paralyzed and arrest at the 2F stage. In the following paragraphs, we discuss mostly the early phase of elongation which occurs prior to muscle contraction onset.

Pharmacological and genetic studies have proved the critical role of actomyosin contractility during the early elongation. Inhibition of actin polymerization with cytochalasin-D prior to the 1.5F stage blocks elongation, whereas application at later stage causes embryos to retract to their pre-elongation state[1]. Non-muscle myosin II activation is regulated through phosphorylation and dephosphorylation of the regulatory light chain MLC-4 by the LET-502/Rho-binding kinase and MEL-11/Myosin phosphatase, respectively[2;3;4]. LET-502, the effector of the Rho GTPase RHO-1, can be activated and inactivated by the *C. elegans* RhoGEF (Guanine Exchange Factors) RHGF-2, and RhoGAP (GTPase Activating Protein) RGA-2[5;6], respectively. Mutations affecting myosin II or its activation, such as MLC-4 and NMY-1/Non-muscle Myosin II heavy chain, RHGF-2/RhoGEF, LET-502/ROCK, lead to hypo-elongation, whereby embryos arrest earlier than or at the 2F stage[2;4;5;7;8]. By contrast, mutations affecting negative regulators of myosin II, like *mel-11* or *rga-2*, cause embryos to burst during elongation due to increased tension exerted on adherens junctions[3;6]. The two myosin heavy chains, NMY-1 and NMY-2, work redundantly to regulate actomyosin contractility[8]. Although essential during early embryonic development, our data shows that NMY-2 is not required during elongation. Indeed, embryos homozygous for the strong thermosensitive mutant *nmy-2(ne3409)*[9] still elongated normally after shifting to the restrictive temperature (25.5° C, data not show).

Several lines of evidence suggest that seam cells generate most of the actomyosin forces, while the DV cells may remain passive. First, the myosin II regulatory light chain MLC-4 is mainly required in seam cells[4]. Second, MLC-4, MLC-5/myosin essential light chain and NMY-1 are higher expressed in seam cells[4;7;8]. Third, rescue experiments have shown that the positive regulator of contractility RHGF-2/RhoGEF is required only in seam cells, whereas the negative regulator RGA-2/RhoGAP acts specifically in DV cells[5;6]. Thus, all the players of acto-myosin regulation pathway promote a high contractility in seam cells and keep a low contractility in DV cells.

Although the myosin II activity is crucial in seam cells, the phenotypes of several mutants affecting junctional proteins, which are thought to anchor actin bundles[10], show an important role of actin bundles in DV epidermal cells during elongation. In particular, zygotic *hmp-1/α-catenin* mutants, in which actin bundles detach from the junctional belt, show bulges and cannot elongate. Similarly, loss of ZOO-1/ZO-1 and VAB-9/Claudin homologues affects actin bundle organization in DV cells, leading to deformities and an incomplete elongation[11;12].

In summary, the epidermal actomyosin network is essential for the early elongation phase of *C. elegans* embryo.

2 Supplementary SI2: The *C. elegans* embryonic epidermis is under biaxial stress loading along the AP and DV directions

Despite the fact that a biological material is in general viscoelastic[13], the elastic aspect of *C. elegans* embryos seems to be more important. Indeed, inhibition of actin polymerization with cytochalasin-D induces a retraction of the embryo to nearly its original length[1], like a spring after force release. Thus, we used an elastic model to describe *C. elegans* embryonic deformation. In particular, we considered the epidermal cell cortex as an elastic plane. In this section, we examine, for the analysis of laser ablation responses, whether the epidermal cell cortex is subjected to biaxial stress loading (stress along two orthogonal directions) along the AP and DV directions.

If a thin cut is introduced in an infinite isotropic elastic plane under biaxial stress loading (figure SI2a), Theocaris *et al.*[14] have shown that the opening is an ellipse. The authors have shown that, the rotation angle θ between the direction of the cut and the major axis of the opening ellipse, is in general different from zero (figure SI2b). θ is equal to zero when the cuts are parallel to the directions of stress loading or in case of equal tension-tension loading ($\sigma_{xx} = \sigma_{yy} > 0$)[14].

To test if the AP and DV directions are indeed the directions of stress loading for different seam cells (H1, V3, V6, figure 3a) during early elongation, we performed laser cuts in the AP and DV directions and measured the rotation angle θ at equilibrium from the 1.3F to the 1.7F stages. Figure SI2c shows that θ was not significantly different from zero for different magnitudes of stress (figure 3b), consistent with the hypothesis that AP and DV are the principal directions of stress loading. The difference of θ compared to 0 was more important for V6, as we had difficulties to unambiguously determine the AP and DV direction for V6. In conclusion, the epidermal cell cortex can be considered as an elastic plane under biaxial stress loading along the AP and DV directions.

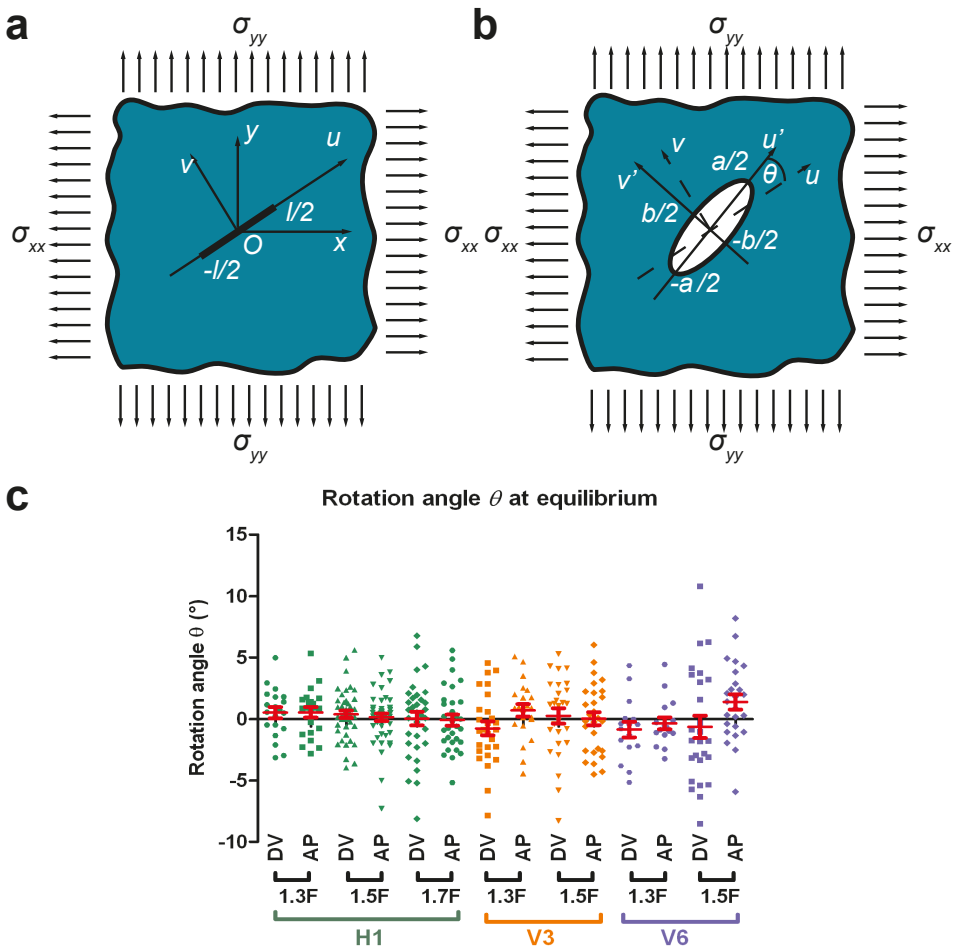

Figure SI2: (**a**) An incision of length l was introduced in an elastic plane under biaxial stress along the x and y directions. The cut was along the u axis with the uv coordinates. (**b**) The shape of the opening at equilibrium was an ellipse[14]. We called u' (of $u'v'$ coordinates) the axis parallel to the major axis of the opening ellipse, which formed an angle θ to the direction of the initial cut. (**c**) The rotation angle θ at equilibrium (measured around 9.5 s after cut) for H1 from the 1.3F to the 1.7F stages and V3 and V6 from the 1.3F to the 1.5F stages. 'DV' and 'AP' mean DV and AP opening, respectively. Red bars show the mean and standard error.

3 Supplementary SI3: Comparison of two methods to analyze laser ablation responses using the recoil dynamics and the cut opening at equilibrium

In order to compare the two analysis methods of laser ablation using the equilibrium shape of the cut opening or the recoil dynamics[15;16], we estimated the initial recoil speed and the relaxation half-time by fitting the relaxation of the cut borders (the minor axis of the cut opening) with the equation:

$$y = y_0 + (Plateau - y_0)(1 - e^{-\gamma t}) \tag{1}$$

where y_0 is the initial width of the cut opening, $Plateau$ is the minor axis of the cut opening at equilibrium and γ is the relaxation rate. The recoil speed can be obtained by taking the derivation of the previous equation versus time:

$$v = \frac{dy}{dt} = (Plateau - y_0)\gamma e^{-\gamma t} \tag{2}$$

Thus, the initial recoil speed is:

$$v_0 = (Plateau - y_0)\gamma \tag{3}$$

The half-time, defined as the time interval needed to reach half of the distance between the initial opening and the $Plateau$, is given by:

$$\tau_{\frac{1}{2}} = \frac{ln(2)}{\gamma} \tag{4}$$

According to the model described in Rauzi *et al.*, Smutny *et al.* and Mayer et al.[15;16;17], the initial recoil speed is proportional to the ratio of the cortical stress σ to the viscosity of the cellular medium η:

$$v_0 \sim \frac{\sigma}{\eta} \tag{5}$$

and the relaxation half-time depends on the ratio of η to the cortex stiffness k:

$$\tau_{\frac{1}{2}} \sim \frac{\eta}{k} \tag{6}$$

The fitting of the equation (1) depends on the initial width of the cut opening y_0. We used here three methods to estimate y_0. First, since the cut opening depends on the actomyosin contractility (figure 2c), we reasoned that y_0 should be close to the opening observed in a mutant where actomyosin contractility is strongly inhibited. Indeed, in *let-502(sb118ts)* mutant, the opening changed very little (figure 2c), which corresponded to a nearly complete inhibition of the early elongation. The smallest opening in *let-502(sb118ts)* mutant was around 0.6 μm (figure 2c). Second, our evaluation of the initial width of the opening using the same setup to photobleach a thin fluorescent layer also gave around 0.6 μm. Finally, we tried to fit the recoil of cut borders using the equation (1) with values of y_0 decreasing from 0.6 μm to 0.2 μm (with 0.1 μm step) and found a decrease of goodness of fit R^2 (supplementary table 2). The goodness of fit R^2 is a fraction between 0 and 1 and higher values indicate better fits (GraphPad Prism 5, *Goodness of fit of nonlinear regression*). Thus, all three approaches indicated that 0.6 μm was a good estimation of the initial width of the cut opening (an example of fit is shown in figure S2). Subsequently, we used $y_0 = 0.6\ \mu m$ to derive the initial recoil speed and the relaxation half-time, and the results are shown in the supplementary table 3.

We found that the relaxation half-time in the AP direction was similar with the one in the DV direction in most of the seam cells examined at different stages (figure SI3a). Since the relaxation time is proportional to the ratio of viscosity over the stiffness of the cortex, and the cytoplasmic viscosity is likely homogeneous within a given cell, the cortex in seam cells is likely isotropic. However it can vary from one cell to another as indicated in the figure SI3a.

Next, we wanted to know if the two methods to analyze the ablation response (based on the cut recoil dynamics and the cut opening at equilibrium) gave consistent results about the stress

magnitude and anisotropy. Since we compared different seam cells (H1, V3, V6) with potentially different material properties (viscosity and stiffness), we multiplied the initial recoil speed by the relaxation half-time to have the stress to stiffness ratio (equations (5,6)). We normalized the previous ratio to the different cut lengths used in the different seam cells (5 μm in H1, 4 μm in V3 and V6), then plotted the resulting values against the cut opening at equilibrium, which also reports the stress over stiffness ratio (figure 2b, figure SI3c). The linear regression strongly suggests that the two methods are in good agreement on the stress magnitude. Moreover, the anisotropy of stress obtained by the two methods showed a linear correlation (SI5d).

In summary, the two methods to analyze laser ablation responses gave results consistent with each other on the magnitude and the anisotropy of stress. The relaxation half-time obtained from recoil dynamics analysis indicated that the seam cell cortex is isotropic.

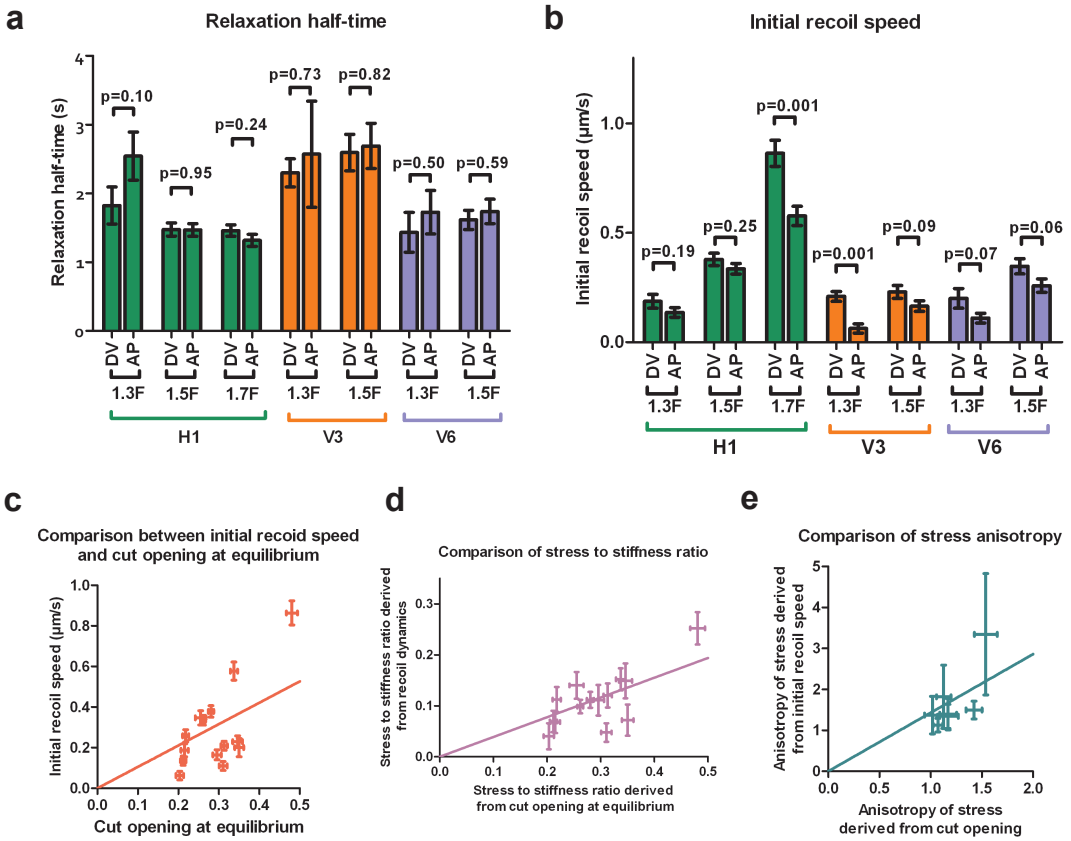

Figure SI3: (**a**) Relaxation half-time and (**b**) initial recoil speed derived from fitting the cut border relaxation using an initial width of cut opening of 0.6 μm, in H1, V3 and V6 from the 1.3F to the 1.7F stages. Z-test, ns, $p > 0.05$; **, $0.001 < p < 0.01$; ***, $p < 0.001$. DV and AP indicate the directions of opening. (**c**) Comparison between the ratio of stress to stiffness derived using the cut recoil dynamics (after normalization to the cut length) and the one derived from the cut opening at equilibrium. (**d**) Comparison of the anisotropy of stress (defined by DV/AP stress) derived from the recoil dynamics and from the cut opening at equilibrium.(**e**) The minor and major axes of cut opening at equilibrium show a linear relationship when the cut length varied from 3 μm to 6 μm. The ablations were performed in H1 at the 1.5F stage. Solid lines show a linear fit. $R^2 > 0.65$. (**f**) The ratio of the minor to major axis of the cut opening at equilibrium calculated from data shown in (**e**).

4 Supplementary SI4: The ratio of the minor to major axis of the cut opening at equilibrium does not depend on the cut length

As predicted by Theocaris *et al.*[14], the minor to major axis ratio of the cut opening should be independent of the cut length. Indeed, the equation for the major axis a over the cut length l of the opening at equilibrium is given as:

$$\frac{a}{l} = \frac{E + \sigma_{xx} - \sigma_{yy}}{E} \tag{7}$$

where σ_{xx} and σ_{yy} are the stresses in the principal loading directions x and y, respectively, which are also the laser cut directions. E is the Young modulus of the plane (figure SI2a-b). Thus, according to the ratio of minor axis to cut length given in figure 2b, the minor to major axis ratio of the ellipse at equilibrium is:

$$\frac{b}{a} = \frac{2\sigma_{yy}}{E + \sigma_{xx} - \sigma_{yy}} \tag{8}$$

and does not depend on the cut length l. Our experimental data fitted well with this prediction as shown in figure SI3e-f. Indeed, when we plotted the minor versus major axes of the opening at equilibrium, we observed a linear relationship (figure SI3e), when the cut length varied from 3 to 6 μm in the seam cell H1, for cuts in both the AP and DV directions. Thus, the minor to major axis ratio is nearly a constant and independent of the cut length (figure SI3f), consistent with the theory of Theocaris *et al.*[14].

5 Supplementary SI5: Modeling of the *C. elegans* embryo as a capped thin-wall pressured vessel and calculation of the anisotropy of stress

The rationale for modeling the *C. elegans* embryo as a thin-wall pressured vessel is given in the main text. To do so, first, we calculated the stress anisotropy for an axisymmetric vessel. We derived the stress anisotropy for the head from this calculation since the head was considered axisymmetric. Second, we calculated the stress anisotropy in the embryo body at the position of the seam cell V3. The body was not axisymmetric due to the important folding of the embryo in the eggshell, but the stress anisotropy can be obtained using a similar method.

5.1 Anisotropy of stress for an axisymmetric thin-wall pressured vessel

We consider an axisymmetric thin-wall pressured vessel with two ends capped. To make a parallel with *C. elegans* embryos, we call the axis of the vessel AP and the circumferential axis DV (figure SI5a). We calculate the anisotropy of stress $\frac{\sigma_{DV}}{\sigma_{AP}}$, where σ_{AP} is the longitudinal (AP) stress and σ_{DV} is the circumferential stress (DV) on the wall.

Let us consider a point Q on the wall for which we calculate $\frac{\sigma_{DV}}{\sigma_{AP}}$ at this point. The tangent at Q in the plane going through Q and the AP axis makes an angle α with AP.

Imagine that we cut the vessel in two parts by a plane going through Q and perpendicular to the AP axis (figure SI5a). The vessel is divided into Ω_1 and Ω_2. The forces applied by Ω_2 on Ω_1 have two components F_1 and F_2 (Figure SI5b): F_1 is the force applied by the wall of Ω_2 on Ω_1, whereas F_2 is the force exerted by the hydrostatic pressure from Ω_2. We have

$$F_1 = \sigma_{AP} 2\pi R h \tag{9}$$

where R is the radius of the vessel at Q; h is the thickness of the wall (epidermis), considered as a constant. F_{1AP} is the component in the AP direction of F_1 and is written as:

$$F_{1AP} = F_1 cos\alpha = \sigma_{AP} 2\pi R h cos\alpha \tag{10}$$

F_{1AP} is balanced by the hydrostatic force F_2 because Ω_1 is at equilibrium

$$F_2 = p\pi R^2 \tag{11}$$

where p is the hydrostatic pressure. By combining the equations (10,11), we have:

$$\sigma_{AP} 2\pi R h cos\alpha = p\pi R^2 \tag{12}$$

$$\Rightarrow \sigma_{AP} = \frac{pR}{2hcos\alpha} \tag{13}$$

Now let's consider a volume element Ω_4 of length Δl with two limiting sections perpendicular to the AP axis, so that Ω_4 is between Ω_3 and Ω_5 (figure SI5c). Imagine that we cut Ω_4 into two halfs Ω_{41} and Ω_{42} (Figure SI5d).

Let's examine an element Δs on the wall of Ω_{41}, at the interface between Ω_3 and Ω_{41}(figure SI5f). The force applied by the wall of Ω_3 to this element is:

$$F_3 = \sigma_{AP}(R_3) h \Delta s = \sigma_{AP}(R_3) h R_3 d\beta \tag{14}$$

where $\sigma_{AP}(R_3)$ means that σ_{AP} is a function of R_3, β is the angle formed by the position of Δs with the Ω_{41}-Ω_{42} interface as shown in figure SI5f. The force applied by Ω_3 on Ω_{41} in the radial direction (figure SI5e-f) is:

$$F_{3R} = F_3 sin\alpha(R_3) = \sigma_{AP}(R_3) h R_3 d\beta sin\alpha(R_3) \tag{15}$$

where $\alpha(R_3)$ means that α is a function of R_3. The force applied by Ω_3 in the direction $\overrightarrow{n}$ perpendicular to the Ω_{41}-Ω_{42} interface (figure SI5f) is:

$$F_{3n} = \int_0^\pi F_{3R} sin\beta d\beta = \int_0^\pi \sigma_{AP}(R_3) h R_3 sin\alpha(R_3) sin\beta d\beta \tag{16}$$

$$= 2\sigma_{AP}(R_3) h R_3 sin\alpha(R_3) \tag{17}$$

If we replace σ_{AP} obtained from the equation (13), we have:

$$F_{3n} = 2\sigma_{AP}(R_3) h R_3 sin\alpha(R_3) = \frac{pR_3^2 sin\alpha(R_3)}{cos\alpha(R_3)} \tag{18}$$

The force F_{5n} exerted by Ω_5 to Ω_3 can be calculated in the same manner. We obtain:

$$F_{5n} = -\frac{pR_5^2 sin\alpha(R_5)}{cos\alpha(R_5)} \tag{19}$$

The resulting force applied by Ω_3 and Ω_5 to Ω_{41} in the $\overrightarrow{n}$ direction can be expressed as :

$$F_{35n} = F_{3n} + F_{5n} = \frac{d}{dR}(\frac{pR^2 sin\alpha(R)}{cos\alpha(R)})\Delta R = 2pRtan\alpha(R)\Delta R + \frac{pR^2}{cos^2\alpha(R)}\frac{d\alpha}{dR}\Delta R \tag{20}$$

The force applied by Ω_{42} to Ω_{41} (figure SI5e-f) in the $\overrightarrow{n}$ direction is :

$$F_{12} = p\Delta l cos\alpha(R) 2R - \sigma_{DV} 2\Delta l h \tag{21}$$

Since Ω_4 is at equilibrium, we have :

$$F_{35n} + F_{12} = 0 \tag{22}$$

Note that

$$\Delta R = \Delta l sin\alpha \tag{23}$$

From the equations (20, 21, 22, 23) we have

$$2pRtan\alpha\Delta l sin\alpha + \frac{pR^2}{cos^2\alpha}\frac{d\alpha}{dR}\Delta l sin\alpha + p\Delta l cos\alpha 2R - \sigma_{DV} 2\Delta l h = 0 \tag{24}$$

$$\Rightarrow \sigma_{DV} = \frac{pRsin^2\alpha}{hcos\alpha} + \frac{pRcos\alpha}{h} + \frac{pR^2sin\alpha}{2hcos^2\alpha}\frac{d\alpha}{dR} = \frac{pR}{hcos\alpha} + \frac{pR^2sin\alpha}{2hcos^2\alpha}\frac{d\alpha}{dR} \tag{25}$$

Thus we obtain the anisotropy of stress on the wall:

$$AS = \frac{\sigma_{DV}}{\sigma_{AP}} = \frac{\frac{1}{cos\alpha} + \frac{Rsin\alpha}{2cos^2\alpha}\frac{d\alpha}{dR}}{\frac{1}{2cos\alpha}} = 2 + R\frac{d\alpha}{dR}tan\alpha \tag{26}$$

We can now calculate the AS for vessels with a particular shape : a sphere, a cylinder and an ellipsoid.

- For a sphere of radius R_0 :

$$R = R_0cos\alpha \tag{27}$$

According to the equation (13), the AP stress is:

$$\sigma_{AP} = \frac{pR_0}{2h} \tag{28}$$

If we take the derivation of the equation (27) with respect to R, we have

$$-R_0sin\alpha\frac{d\alpha}{dR} = 1 \tag{29}$$

$$\Rightarrow R_0cos\alpha tan\alpha\frac{d\alpha}{dR} = -1 \tag{30}$$

$$\Rightarrow Rtan\alpha\frac{d\alpha}{dR} = -1 \tag{31}$$

Combing the previous equation with the equation (26), we have:

$$\Rightarrow AS = \frac{\sigma_{DV}}{\sigma_{AP}} = 1 \tag{32}$$

- For a cylinder : $\alpha = const = 0$

$$AS = \frac{\sigma_{DV}}{\sigma_{AP}} = 2 \tag{33}$$

According to the equation (13), the AP stress is:

$$\sigma_{AP} = \frac{pR}{2h} \tag{34}$$

where R is the radius of the cylinder.

- For an ellipsoid with the major axis a_1 and minor axis a_2 (figure SI5g), we can write the coordinates of point Q in the plane going through Q and AP axis as:

$$\Rightarrow \begin{cases} x = a_1cost \\ y = a_2sint \end{cases} \tag{35}$$

thus

$$tan\alpha = \frac{dy}{dx} = \frac{a_2cost}{a_1(-sint)} = -\frac{a_2}{a_1}cotant \tag{36}$$

$$\frac{d(tan\alpha)}{dt} = (1 + tan^2\alpha)\frac{d\alpha}{dt} = \frac{a_2}{a_1}(1 + cotan^2t) \tag{37}$$

Thus

$$\frac{d\alpha}{dt} = \frac{\frac{a_2}{a_1}(1 + cotan^2 t)}{1 + \frac{a_2^2}{a_1^2} cotan^2 t} = \frac{a_1 a_2}{a_1^2 sin^2 t + a_2^2 cos^2 t} \tag{38}$$

Due to the symmetry of the system, we examine only $t \in [0, \pi]$. We have:

$$R = y = a_2 sint \tag{39}$$

$$\frac{d\alpha}{dR} = \frac{d\alpha}{dt}\frac{dt}{dR} = \frac{a_1 a_2}{(a_1^2 sin^2 t + a_2^2 cos^2 t) a_2 cost} = \frac{a_1}{(a_1^2 sin^2 t + a_2^2 cos^2 t) cost} \tag{40}$$

From equations (36,39,40) we have

$$R\frac{d\alpha}{dR} tan\alpha = \frac{-a_2^2}{a_1^2 sin^2 t + a_2^2 cos^2 t} \tag{41}$$

Thus:

$$AS = \frac{\sigma_{DV}}{\sigma_{AP}} = 2 - \frac{a_2^2}{a_1^2 sin^2 t + a_2^2 cos^2 t} \tag{42}$$

For the middle of the ellipsoid, $y = a_2$ and $x = 0$, $t = \frac{\pi}{2}$, thus

$$AS = \frac{\sigma_{DV}}{\sigma_{AP}} = 2 - \left(\frac{a_2}{a_1}\right)^2 \tag{43}$$

According to the equation (13), the AP stress at the middle of the ellipsoid is:

$$\sigma_{AP} = \frac{p a_2}{2h} \tag{44}$$

Note that the radial stress on the wall is $-p$. Since the wall is thin, i.e $h << R$, we expect that the radial stress is much smaller than the AP and DV stress on the wall for a sphere, an ellipsoid or a cylinder.

5.2 Anisotropy of stress for the body seam cell V3 of *C. elegans* embryo

For the seam cell V_3 at the 1.3F and 1.5F stages, there is an important curvature of the embryo in the ventral part (figure SI5h). We cut a part of the embryo going through V3 and the dorsal part of V3 (dash line, figure SI5h) and approximate that the resulting half-section as half a cylinder (figure SI5i).
The force equilibrium for this part of the embryo in the circumferential direction (figure SI5i) is written as:

$$\sigma_{DV}^{V3} 2hL = p2R_2 L \tag{45}$$

(force generated by circumferential stress on the wall = force due to the hydrostatic pressure), where σ_{DV}^{V3} is the DV stress at V3, h is the thickness of the epidermis, R_2 is the radius at $V3$, L is the length of the region considered. Thus:

$$\sigma_{DV}^{V3} = \frac{pR_2}{h} \tag{46}$$

For H1 in the head, if we considered the head as a sphere, the DV and the AP stresses are the same and is given as (equations 28, 32):

$$\sigma_{DV}^{H1} = \sigma_{AP}^{H1} = \frac{pR_1}{2h} \tag{47}$$

where R_1 is the head radius. If the AP stress is the same for H1 and V3, then the anisotropy of stress at V3 is

$$AS = \frac{\sigma_{DV}^{V3}}{\sigma_{AP}^{H1}} = \frac{\frac{pR_2}{h}}{\frac{pR_1}{2h}} = 2\frac{R_2}{R_1} \tag{48}$$

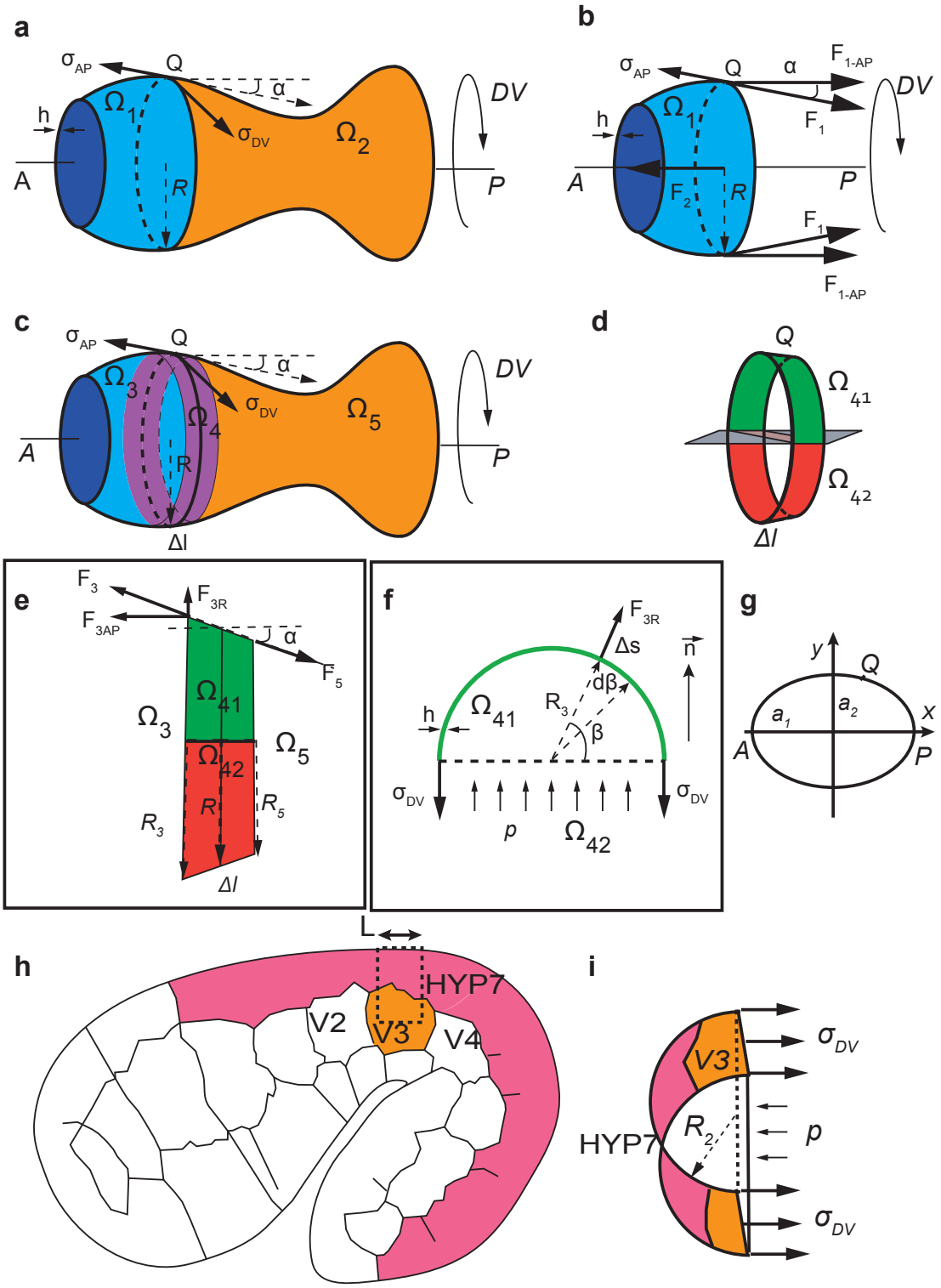
a
σAP
Q
α
h
Ω1
σDV
Ω2
A
R
DV
P
b
σAP
Q
α
F1-AP
DV
h
Ω1
F1
A
F2
R
P
F1
F1-AP
c
σAP
Q
α
Ω3
σDV
Ω5
Ω4
A
R
DV
P
Δl
d
Q
Ω41
Ω42
Δl
e
F3
F3R
F3AP
α
F5
Ω41
Ω3
Ω5
Ω42
R
R5
R3
Δl
f
F3R
Δs
n
dβ
R3
h
Ω41
β
σDV
σDV
p
Ω42
g
y
Q
a1
a2
x
A
P
L
h
HYP7
V2
V3
V4
i
σDV
V3
HYP7
R2
p
σDV

Figure SI5

6 Supplementary SI6: The Hooke's law written for seam and DV epidermal cells

In this section, we further detail how we used the Hooke's law to describe the deformation of the seam and DV epidermal cells.

6.1 Supplementary SI6A: The Hooke's law written for seam cells

The Hooke's law for the deformation of seam cells is given by:

$$\epsilon^s_{AP} = \frac{\Delta L^s_{AP}}{L^s_{0AP}} = \frac{\sigma^s_{AP}}{E} - \nu\frac{\sigma^s_{DV}}{E} = -\frac{\sigma^s_{AP}}{E}(\nu AS - 1) \tag{49}$$

$$\epsilon^s_{DV} = \frac{\Delta L^s_{DV}}{L^s_{0DV}} = \frac{\sigma^s_{DV}}{E} - \nu\frac{\sigma^s_{AP}}{E} = -\frac{\sigma^s_{AP}}{E}(\nu - AS) \tag{50}$$

Here we supposed that the embryonic cortex material property is isotropic with a Young modulus E. ϵ^s_{AP} and ϵ^s_{DV} are the strain (which is equal to the relative length change) along the AP and DV directions, respectively; ΔL^s_{AP} and ΔL^s_{DV} are the length change, L^s_{0AP} and L^s_{0DV} are the initial length along the AP and DV directions, respectively. Positive values of ϵ^s_{AP} or ϵ^s_{DV} correspond to an increase in length (or extension), whereas negative values correspond to a decrease in length (shrinking). σ^s_{AP} and σ^s_{DV} are the stress along the AP and DV directions, respectively. Positive values of σ^s_{AP} or σ^s_{DV} correspond to tensile stress, whereas negative values correspond to contractile stress. ν is the Poisson's ratio describing the shrinking in the AP direction when tensile stress is applied in the DV direction, and vice-versa. Here we omit the stress along the radial direction, since it is much smaller than the AP and DV stress for a thin-wall vessel (supplementary SI5). AS is the stress anisotropy which equals to the DV to AP stress ratio.

$$AS = \frac{\sigma^s_{DV}}{\sigma^s_{AP}} \tag{51}$$

If we have an isotropic spherical embryo covered with contractile seam cells ($AS = 1$), the embryo would not deform due to its incompressibility and symmetry: $\epsilon^s_{AP} = 0$ and $\epsilon^s_{DV} = 0$. From this we derived that $\nu = 1$. We can thus rewrite the previous equations (49, 50) as:

$$\epsilon^s_{AP} = -\frac{\sigma^s_{AP}}{E}(AS - 1) \tag{52}$$

$$\epsilon^s_{DV} = -\frac{\sigma^s_{AP}}{E}(1 - AS) \tag{53}$$

6.2 Supplementary SI6B: The Hooke's law written for DV epidermal cells

As the DV epidermal cells have different stiffnesses along the AP and DV directions, the stress-strain relationship along the AP and DV axes can be written:

$$\epsilon_{AP} = \frac{\Delta L_{AP}}{L_{0AP}} = \frac{\sigma_{AP}}{E_{AP}} - \nu_1\frac{\sigma_{DV}}{E_{DV}} \tag{54}$$

$$\epsilon_{DV} = \frac{\Delta L_{DV}}{L_{0DV}} = \frac{\sigma_{DV}}{E_{DV}} - \nu_2\frac{\sigma_{AP}}{E_{AP}} \tag{55}$$

where ϵ_{AP} and ϵ_{DV} are the strain (which is equal to the relative length change) along the AP and DV axes, respectively; ΔL_{AP} and ΔL_{DV} are the length change, L_{0AP} and L_{0DV} are the initial length of the cell in the the AP and DV directions, respectively. Positive values of ϵ_{AP} or ϵ_{DV} correspond to an increase in length (or extension), whereas negative values correspond to a decrease in length (shrinking) of the cells. σ_{AP} and σ_{DV} are the stress along the AP and DV directions, respectively. Positive values of σ_{AP} or σ_{DV} correspond to tensile stress, whereas negative values correspond to contractile stress. ν_1 and ν_2 are Poisson's ratios.

Since the head is considered axisymmetric, we have:

$$AS = \frac{\sigma^s_{DV}}{\sigma^s_{AP}} = \frac{\sigma_{DV}}{\sigma_{AP}} \tag{56}$$

and replace

$$\omega = \frac{E_{DV}}{E_{AP}} \tag{57}$$

we have

$$\epsilon_{AP} = \frac{\sigma_{AP}}{E_{AP}}\left(1 - \nu_1 \frac{AS}{\omega}\right) \tag{58}$$

$$\epsilon_{DV} = \frac{\sigma_{DV}}{E_{DV}}\left(1 - \nu_2 \frac{\omega}{AS}\right) \tag{59}$$

While the CB model (see supplementary SI7,section 8.4) seems to be appropriate to describe fiber-reinforced material in extension, its application is questionable to describe the shrinking in the fiber direction. It is known for many fiber-reinforced composites to exhibit different stiffnesses in response to extension and compression[18;19]. It is also known for biological polymers, such as actin filaments, that they can have different mechanical properties under tensile or compressive stress, as actin filaments buckle under compression[20]. The use of Poisson's ratios for fiber-reinforced material in compression is arguable, since the symmetry of stiffness (or compliance) matrix may not be satisfied[18]. Given that the DV cells decrease their length in the fiber (DV) direction (figure 3e), the fibers should be under compression. For this reason, we suggest that the DV epidermal cells must have an active mechanism to adjust the actin bundle length to the cell shrinkage along the DV direction, in order to maintain the reinforcement properties.

7 Supplementary SI7: Cracks opening in orthotropic and fiber-reinforced planes

7.1 Introduction

This supplementary gives the proofs of the various relations used in the main paper to extract the residual stresses in the epithelial cells. Exhibiting oriented actin cables, the epithelium can be considered as a thin anisotropic soft layer. The correct description of the epithelium behaviour under strong deformations is achieved via hyper-elasticity. However, the determination of a crack-shape in nonlinear elastostatic remains challenging and is not achieved to the best of our knowledge. It is why we assume first a linear orthotropic planar material and solve the geometry of the crack by potential functions[21;22], following the pioneering contributions of Muskkhelishvili[23], Suo[24], Theocaris *et al.*[14] and Yoffe[25]. In the following, the shape of the crack is given, under simultaneous tension imposed far away along Ox and Oy, including also shear stresses (combined Mode I and II of fracture). Then, we present the model for fiber soft material, which is a better representation for living matter. Aiming to estimate residual stresses from the shape aperture, we identify the correspondence between the linear elastic coefficients of anisotropic elasticity and the parameters of a fiber model, at low strains.

7.2 Fracture in orthotropic linear elasticity

In material sciences, a common choice of elastic coefficients for orthotropic samples consists in the definition of Young moduli affected to each axis and Poisson ratios defined for each pair of orientation, in addition to shear moduli (equivalent to the second Lamé coefficients[21] μ) . In case of plane stress elasticity, the equivalent Hooke's law is reduced to six independent coefficients:

$$\begin{cases} u_{xx} = \frac{1}{E_x}(\sigma_{xx} - \nu_{xy}\sigma_{yy}); \quad u_{yy} = -\frac{\nu_{xy}}{E_x}\sigma_{xx} + \frac{\sigma_{yy}}{E_y} \\ u_{zz} = -\frac{\nu_{xz}}{E_x}\sigma_{xx} + \frac{\nu_{yz}}{E_y}\sigma_{yy}; \quad u_{xy} = \frac{1}{2\mu_{xy}}\sigma_{xy} \end{cases} \tag{60}$$

The incompressibility condition: $\Sigma_i u_{ii} = 0$ involves the third components of the deformation u_{zz}, leading to: $\nu_{xz} = \nu_{yz} = 1$, so finally 4 elastic independent coefficients are required. When the loads are applied at the border of the sample, the two in-plane components of the equilibrium condition Div $\sigma = 0$:

$$\frac{\partial \sigma_{xx}}{\partial x} + \frac{\partial \sigma_{xy}}{\partial y} = 0 \quad \text{and} \quad \frac{\partial \sigma_{xy}}{\partial x} + \frac{\partial \sigma_{yy}}{\partial y} = 0, \tag{61}$$

are automatically satisfied by the definition of the Airy potential[21]: $U(x, y)$:

$$\sigma_{xx} = \frac{\partial^2 U}{\partial y^2}; \quad \sigma_{xy} = -\frac{\partial^2 U}{\partial x \partial y}; \quad \sigma_{yy} = \frac{\partial^2 U}{\partial x^2} \tag{62}$$

Taking into account the Hooke's law, Eq.(60), one recovers the usual forth order partial differential equation for U:

$$\frac{\partial^4 U}{\partial x^4} + 2\rho\Lambda^{1/2}\frac{\partial^4 U}{\partial x^2 \partial y^2} + \Lambda\frac{\partial^4 U}{\partial y^4} = 0 \tag{63}$$

where $\Lambda = E_y/E_x$ and $\rho = \frac{1}{2}\sqrt{\Lambda}(E_x/\mu_{xy} - 2\nu_{xy})$. For isotropic materials, $\Lambda = \rho = 1$, since the second Lamé coefficient (related to the Young modulus E and to the Poisson ratio ν) reads: $\mu = E/(2(1+\nu))$. In the isotropic case and in the context of fracture, Eq.(63) has been solved[23] with the help of holomorphic functions and complex analysis, in the case of plane-stress or plain strain elasticity and in Mode I (uniaxial loading, perpendicular to the crack direction). The method has been extended to bi-axial loading and arbitrary crack orientation by Theocaris *et al*[14] using the same strategy. Coming back to the anisotropic case and as pointed by Suo[24], the theoretical analysis differs according to the ρ value. However, to the best of our knowledge, the shape of a crack of finite length has not been determined before, for an orthotropic material. Since we are concerned with $\rho < 1$, proofs will be given for $-1 < \rho < 1$ and the results for the shape crack will be simply mentioned without demonstration for arbitrary ρ.

7.3 Definition of two complex functions

Eq.(63) is an even quartic partial differential equation which can be solved by 2 holomorphic functions $\tilde{F}(z_1)$ and $\tilde{G}(z_2)$ where:

$$z_1 = x + \Lambda^{-1/4}(m + In)y; \quad z_2 = \Lambda^{-1/4}(-m + In)y; \quad n = \sqrt{(1+\rho)/2} \quad \text{and} \quad m = \sqrt{(1-\rho)/2}. \tag{64}$$

This treatment is inspired from the work of Yoffe[25] for elasto-dynamic cracks in mode I and differs slightly from the work of Muskkhelishvili[23] and Lekhnitskii[26], more fancy but much less intuitive. In the following, the formulation via complex potentials can be checked at each step by elementary calculations. Each stress component σ_{ij} also verifies Eq.(63) and can be written as:

$$\sigma_{yy} = 2Re[F'(z_1) + G'(z_2)]; \;\; \sigma_{xy} = -2Re[\mu_1 F'(z_1) + \mu_2 G'(z_2)]; \;\; \sigma_{xx} = 2Re[\mu_1^2 F'(z_2) + \mu_2^2 G'(z_2)] \tag{65}$$

where $F(z) = d\tilde{F}(z)/dz$. The reader can check easily that the two components of the equilibrium equation (61) are verified. A standard choice for $F'(z_1)$ and $G'(z_2)$ for a crack lying on the x-axis between $-a < x < a$ is:

$$F'(z_1) = (A_1 + iA_2)\frac{z_1}{\sqrt{z_1^2 - (l/2)^2}} + B_1 + iB_2 \;\; \text{and} \;\; G'(z_2) = (C_1 + iC_2)\frac{z_2}{\sqrt{z_1^2 - (l/2)^2}} + D_1 + iD_2 \tag{66}$$

where the 8 constants are real and will be determined by the boundary conditions on the crack lips and the loads far from the crack. On the lips, we have the cancellation of σ_{xy} and σ_{yy} and both square-roots in Eq.(66) are imaginary, so it reads:

$$\begin{cases} \sigma_{yy} = 0 \Longrightarrow B_1 = -D_1 \quad \text{and} \quad C_2 = -A_2, \\ \sigma_{xy} = 0 \Longrightarrow C_1 = (C_2 - A_2)m/n - A_1 \quad \text{and} \quad D_2 = (B_1 - D_1)m/n - B_2 \end{cases} \tag{67}$$

Eliminating the solid rotation at infinity leads to $B_1 = -n(mA_2 + nA_1)$, thus giving a fith relationship. It remains to evaluate the 3 stress components at infinity $\sigma_{yy}^\infty, \sigma_{xy}^\infty, \sigma_{xx}^\infty$ and we obtain:

$$A_1 = \frac{1}{4}\big(\sigma_{yy}^\infty - \Lambda^{1/4}\sigma_{xy}^\infty/m\big), \quad A_2 = -\frac{n}{4m}\sigma_{yy}^\infty, \quad B_2 = \frac{1}{8mn}\big(-\sqrt{\Lambda}\sigma_{xx}^\infty + \sigma_{yy}^\infty + 2mn^2\Lambda^{1/4}\sigma_{xy}^\infty\big) \quad (68)$$

Finally, taking into account the first relationship of the Hooke's law, Eq.(60), knowing that $u_{xx} = \partial u/\partial x$, one can find the horizontal displacement on the lips by quadrature :

$$u_\pm = \frac{2}{\sqrt{E_x E_y}}\{\frac{1}{2}(\sigma_{xx}^\infty \Lambda^{1/2} - \sigma_{yy}^\infty)x \pm n\Lambda^{1/4}\sigma_{xy}^\infty\sqrt{(l/2)^2 - x^2}\} \quad (69)$$

The determination of the vertical displacement is more subtile since v comes from the shear relation: $\partial v/\partial x = -\partial u/\partial y + \sigma_{xy}/\mu_{xy}$, and we obtain after elimination of solid rotation,

$$v_\pm = \frac{2n}{E_x^{1/4}E_y^{3/4}}\{n\Lambda^{1/4}\sigma_{xy}^\infty x \pm \sigma_{yy}^\infty\sqrt{(l/2)^2 - x^2}\} \quad (70)$$

In pure tensional loading, σ_{xy}^∞, calling β the ratio between the imposed vertical tension and the horizontal one: $\beta = \sigma_{xx}/\sigma_{yy}$, we obtain:

$$u_\pm = \Lambda^{1/2}\frac{\sigma_{yy}^\infty}{E_2}(\beta\Lambda^{1/2} - 1)x \quad \text{and} \quad v_\pm = \pm 2n\Lambda^{1/4}\frac{\sigma_{yy}^\infty}{E_y}\sqrt{(l/2)^2 - x^2} \quad (71)$$

Even if the demonstration given here is for $\rho < 1$, a slightly different treatment can be achieved for $\rho = 1$ and $\rho > 1$ but Eq.(69) and (70) and Eq.(71) remain valid with the same definition of $n = \sqrt{(1+\rho)/2}$ and Λ.

Linear elasticity allows to solve exactly problems of interest in two dimensions, but it is not fully adapted to living matter which responds differently to low and high stresses. Indeed, in linear elasticity, the material answers linearly to the forcing while for living tissues, we know that large strains resist to the forcing mostly because of the fibers present in the tissue. Finite elasticity for soft materials is a fast-developing domain presently but it is technically more difficult. In particular, no exact crack solutions exist. Nevertheless, it presents a better description of the elastic energy: it is the reason why we present hereafter the fiber model in finite elasticity, which is probably more adapted to the epithelium we are considering.

7.4 Fiber model in finite elasticity

For a fibrous material, the elastic energy density W is chosen as the superposition of the energy of a gelatinous matrix W_{nH} (most often, the neo-Hookean or the Monney-Rivlin model[29]) and a fiber contribution[27;28;30]. Different models exist, more or less complicated, based on the experimental responses of fibrous samples to stresses: muscles, arteries, and on required mathematical properties. We select a model which has the property to behave likely in tension or compression, that is the CB model[27;28], contrary to other models such the $G-O-H$ model[30] which gives a non symmetric answer in tension and compression. As shown in the Lecture[31], the CB model eliminates unexpected singularities such as the one obtained at low strains in dispersion relations. Choosing a neo-Hookean matrix,

$$W_{nH} = \frac{\mu_0}{2}\Big(\lambda_1^2 + \lambda_2^2 + \lambda_3^2 - 3) \quad (72)$$

where W_{nH} is function only of the first invariant I_1 =tr$[\mathbf{F}\mathbf{F}^\mathbf{T}]$, ($\mathbf{F}$ being the strain tensor, defined by $F_{ij} = \partial u_i/\partial u_j$), contrary to the Mooney-Rivlin model which incorporates also the second invariant I_2. We choose the fiber contribution[27;28] as:

$$W_{CB} = \frac{\mu_0}{2}K\{2\kappa(\lambda_1^2 + \lambda_2^2 + \lambda_3^2 - 3) + (1 - 3\kappa)(\lambda_2^2 + \frac{1}{\lambda_2^2}) - 2\} \quad (73)$$

where κ is a dispersion coefficient when the fibers are disordered[28] and K is directly connected to the elasticity of the fibers compared to the elasticity of the matrix. For simplicity, we put $\kappa = 0$ hereafter. Since we cannot solve the crack problem for a nonlinear sample, our plan is to consider the low strain limit and relate the coefficients Λ and ρ which are responsible for the crack shape to the coefficients μ_0 and K of nonlinear elasticity. Considering plane-stress elasticity, minimization of the elastic energy concerns the free energy under the constrain of incompressibility and the condition that the Cauchy stress components σ_{iz} cancel.

$$G = \int dX_1 dX_2 dX_3 \{W(\lambda_1, \lambda_2, \lambda_3) - 3) - P\lambda_3 J_{2D}\}, \tag{74}$$

where J_{2D} represents the Jacobian in $2D$ and P is a Lagrange multiplier. Minimization with respect to the strain in the third direction gives:

$$P = \frac{1}{J_{2D}} \frac{\partial W}{\partial \lambda_3} = \lambda_3 \frac{\partial W}{\partial \lambda_3} \tag{75}$$

7.5 Fiber versus orthotropic elasticity in extension

The correspondence between the anisotropic coefficients of the linear elasticity and the finite fiber elasticity is possible at small values of the strain such that $\epsilon_i = |\lambda_i - 1| << 1$. For plane-stress elasticity, the Cauchy stress leads to:

$$\sigma_i = \lambda_i \frac{\partial W}{\partial \lambda_i} - P = \lambda_i \frac{\partial W}{\partial \lambda_i} - \lambda_3 \frac{\partial W}{\partial \lambda_3} \tag{76}$$

Expanding all λ_i for weak deformations, we derive without difficulty, for the C-B model:

$$\epsilon_1 = \frac{1}{\mu_0} \frac{1+K}{3+4K} \left(\sigma_1 - \frac{1}{2(1+K)} \sigma_2 \right) \quad \text{and} \quad \epsilon_2 = \frac{1}{\mu_0} \frac{1}{3+4K} (\sigma_2 - \frac{1}{2}\sigma_1) \tag{77}$$

Comparison with the orthotropic Hookean law, Eq.(60), in-plane stress elasticity gives:

$$E_x = \mu_0 \left(\frac{3+4K}{1+K} \right); \quad E_y = \mu_0(3+4K); \quad \Lambda = 1+K; \qquad \text{and} \quad \nu_{xy} = \frac{1}{2(1+K)} \tag{78}$$

If we call the stiffness of the matrix (without fiber) E_0, we have

$$E_0 = 3\mu_0 \tag{79}$$

and

$$E_x = \frac{E_0}{3} \left(\frac{3+4K}{1+K} \right); \quad E_y = \frac{E_0}{3}(3+4K) \tag{80}$$

7.6 Fiber versus orthotropic elasticity in the case of shear deformation

To complete the set of coefficients, we need the shear coefficient μ_{xy} so we treat a pure shear deformation such as: Then, the new coordinates in the current deformation are

$$x = X + \Gamma Y; \quad y = Y \quad z = Z \tag{81}$$

giving the deformation tensor $\mathbf{F}$, the left Cauchy -Green tensor[29] $\mathbf{F}\mathbf{F}^{\mathbf{T}}$ and the Cauchy stress tensor[31] σ

$$\mathbf{F} = \begin{bmatrix} 1 & \Gamma & 0 \\ 0 & 1 & 0 \\ 0 & 0 & 1 \end{bmatrix}; \mathbf{F}\mathbf{F}^{\mathbf{T}} = \begin{bmatrix} 1+\Gamma^2 & \Gamma & 0 \\ \Gamma & 1 & 0 \\ 0 & 0 & 1 \end{bmatrix}; \sigma = \begin{bmatrix} 1 & \Gamma\mu_0(1+2K) & 0 \\ \Gamma\mu_0(1+2K) & 0 & 0 \\ 0 & 0 & 0 \end{bmatrix} \tag{82}$$

where σ is evaluated according to the following expression[31]

$$\sigma = \mu_0(\mathbf{F}\mathbf{F}^{\mathbf{T}} - \mathbf{I}) + \mu_0 K\{(\mathbf{F}\cdot\mathbf{M}) \otimes (\mathbf{F}\cdot\mathbf{M}) - (\mathbf{F}^{-\mathbf{T}}\cdot\mathbf{M}) \otimes (\mathbf{F}^{-\mathbf{T}}\cdot\mathbf{M})\} \tag{83}$$

restricted to the linear approximation for weak value of the shear strain Γ. So the shear modulus μ_{xy} of the orthotropic material is then:

$$\mu_{xy} = \mu_0(1+2K) = E_x \frac{1+K}{3+4K}(1+2K) \tag{84}$$

which allows the calculation of the coefficient ρ introduced in Eq.(63):

$$\rho = \sqrt{\Lambda}(\frac{E_1}{2\mu_{xy}} - \nu_{xy}) = \frac{\sqrt{\Lambda}}{2(1+K)}(\frac{3+4K}{1+2K} - 1) = \frac{\sqrt{1+K}}{1+2K} \tag{85}$$

7.7 How to evaluate the residual stress from the crack opening

When we cut a fibrous sample, perpendicularly to the direction of the fibers, we obviously change the structure locally and also the elastic properties along the crack. It is not sure that the CB model describes the correct elasticity since the new aperture is free from fibers. Perhaps a better approximation for the shape aperture is an isotropic elasticity. However, far from the crack of length l, on a distance larger than l, the stresses reach the value at infinity so σ_{yy} and the sample is fibrous. The CB model is an approximation but also the isotropic model and the truth is perhaps between these extremes. In addition, we consider an infinite sample in all directions Ox, Oy which implicitly assumes that the crack length is small compared to the epithelium size. The the opening ellipse, in the isotropic approximation is then:

$$b_y = 4\frac{\sigma_{yy}}{3\mu_0}\sqrt{(l/2)^2 - x^2} \tag{86}$$

with a crack on the x axis having a length l. The minor axis of the opening is then:

$$b_y = 2\frac{\sigma_{yy}}{3\mu_0}l = 2\frac{\sigma_{yy}}{E_0}l \tag{87}$$

Considering now that we cut the sample along the Oy direction then the cut opening ellipse is

$$b_x = 4n\Lambda^{-1/4}\frac{\sigma_{xx}^{\infty}(1+K)}{\mu_0(3+4K)}\sqrt{(l/2)^2 - y^2} \tag{88}$$

where n is not modified and varies between 1 and $1/2$ for increasing stiffness. The minor axis of the opening is:

$$b_x = 2n\Lambda^{-1/4}\frac{\sigma_{xx}^{\infty}(1+K)}{\mu_0(3+4K)}l = 2n\Lambda^{-1/4}\frac{\sigma_{xx}^{\infty}}{E_x}l \tag{89}$$

8 Supplementary SI8: Modeling the DV epidermis as an orthotropic material

As outlined in the main text, we could also have modeled the DV epidermis as an orthotropic material (with different stiffnesses in orthogonal directions). In this section, we argued that doing so is not compatible with the elongation of the embryo.

We modeled the DV epidermis as an orthotropic material with two principal Young moduli along the DV and AP directions E_{DV} and E_{AP}, respectively. We suppose that the stresses σ_{DV} and σ_{AP} are applied along the DV and AP directions, respectively, and there is no shear stress. The opening in the DV and AP directions is given by the equation (70):

$$\frac{b_{DV}}{l} = 2n\left(\frac{E_{DV}}{E_{AP}}\right)^{\frac{1}{4}}\left(\frac{\sigma_{DV}}{E_{DV}}\right) \tag{90}$$

$$\frac{b_{AP}}{l} = 2n \left(\frac{E_{AP}}{E_{DV}}\right)^{\frac{1}{4}} \left(\frac{\sigma_{AP}}{E_{AP}}\right) \tag{91}$$

where b_{DV} and b_{AP} are the minor axis of the cut opening in the DV and AP directions, respectively; l is the initial cut length. n is the parameter given in the equation (64).

To obtain the DV/AP Young moduli ratio, if we divide the opening in the DV to the AP direction (same cut length), then we have :

$$\frac{b_{DV}}{b_{AP}} = \left(\frac{E_{AP}}{E_{DV}}\right)^{\frac{1}{2}} \left(\frac{\sigma_{DV}}{\sigma_{AP}}\right) = \left(\frac{E_{AP}}{E_{DV}}\right)^{\frac{1}{2}} AS \tag{92}$$

From the measurement of the AP and DV opening and given the same anisotropy of stress AS in the HYP7 cell as in the H1 cell, we can derive the ratio of DV/AP Young moduli $\frac{E_{DV}}{E_{AP}}$.

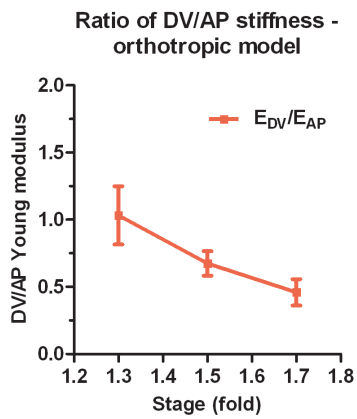

Figure SI8: Ratio of DV/AP Young moduli calculated from the orthotropic model for the DV epidermis.

Figure SI8 shows that the ratio of DV/AP Young moduli, calculated from the orthotropic model, decreased as the embryo elongated. This ratio became less than 1 after the 1.3F stage. Since the activity of myosin II in the DV epidermis is low, the DV cells are likely submitted to tensile stress from the seam cells. According to the Hooke's law written for DV cells (supplementary SI6B) and given a positive tensile stress on the DV cells, a decrease in the DV/AP Young moduli ratio (ω) should decrease the AP length and increases the DV length. Thus, a decrease in the DV/AP Young moduli ratio as given by the orthotropic model would hinder the elongation of the DV cells in the AP direction and thus of the embryo as a whole, and be inconsistent with the contribution of the DV cells during *C. elegans* embryo elongation (figure 3e).

9 Supplementary SI9: Calculation of the ratio of Young moduli between the seam cell H1 and the head HYP7 cell matrix

To compare the material properties (Young modulus) between the seam cell H1 and the head HYP7 cell matrix (without fibers), we made use of the opening in the DV direction when performing laser cuts in these cells. The DV opening in the seam cell H1 is given as indicated in figure 2b:

$$\frac{b_{DV}^{H1}}{l} = 2\frac{\sigma_{DV}^{H1}}{E} \tag{93}$$

where b_{DV}^{H1} is the minor axis of the cut opening at equilibrium, l is the cut length, σ_{DV}^{H1} is the DV stress in H1 and E is the Young modulus of H1. The head HYP7 cell behaved like an isotropic

medium with a Young modulus E_0 with cuts perpendicular to the actin fibers (DV opening). Thus, the DV opening in the head HYP7 cell is given as:

$$\frac{b_{DV}^{HYP7}}{l} = 2\frac{\sigma_{DV}^{HYP7}}{E_0} \tag{94}$$

where b_{DV}^{HYP7} is the minor axis of the cut opening at equilibrium, l is the cut length, σ_{DV}^{HYP7} is the DV stress in the head HYP7 cell. Given their adjacent position (figure 3d), H1 and head HYP7 should be under the same DV stress:

$$\sigma_{DV}^{H1} = \sigma_{DV}^{HYP7} \tag{95}$$

Thus:

$$\frac{b_{DV}^{HYP7}}{l} = 2\frac{\sigma_{DV}^{HYP7}}{E_0} = 2\frac{\sigma_{DV}^{H1}}{E}\frac{E}{E_0} = \frac{b_{DV}^{H1}}{l}\frac{E}{E_0} \tag{96}$$

When we plotted the DV opening in the head HYP7 cell versus the DV opening in H1, the slope gives us the ratio of Young moduli $\frac{E}{E_0}$.

10 Supplementary SI10: Calculation of K and DV/AP Young moduli ratio for a fiber-reinforced material

For a fiber-reinforced material, from the equations (78, 85, 87, 89), we have:

$$\frac{b_{DV}}{b_{AP}} = \frac{(3+4K)\sqrt{2}}{3(1+\frac{\sqrt{1+K}}{1+2K})^{\frac{1}{2}}(1+K)^{\frac{3}{4}}}\frac{\sigma_{DV}}{\sigma_{AP}} = \frac{(3+4K)\sqrt{2}}{3(1+\frac{\sqrt{1+K}}{1+2K})^{\frac{1}{2}}(1+K)^{\frac{3}{4}}}AS \tag{97}$$

where b_{DV} and b_{AP} are the minor axis of the DV and AP openings (we used the same cut length l), respectively; AS is the anisotropy of stress and K is the fiber contribution factor. Since we can measure the openings, given the anisotropy of stress, we can calculate K. We can easily derive the DV/AP Young moduli ratio according to the equation (78):

$$\omega = \frac{E_{DV}}{E_{AP}} = 1 + K \tag{98}$$

References

[1] Priess, J.R. & Hirsh, D.I. Caenorhabditis elegans morphogenesis: the role of the cytoskeleton in elongation of the embryo. *Developmental biology* **117**, 156-173 (1986).

[2] Wissmann, A., Ingles, J., McGhee, J.D. & Mains, P.E. Caenorhabditis elegans LET-502 is related to Rho-binding kinases and human myotonic dystrophy kinase and interacts genetically with a homolog of the regulatory subunit of smooth muscle myosin phosphatase to affect cell shape. *Genes Dev* **11**, 409-422 (1997).

[3] Wissmann, A., Ingles, J. & Mains, P.E. The Caenorhabditis elegans mel-11 myosin phosphatase regulatory subunit affects tissue contraction in the somatic gonad and the embryonic epidermis and genetically interacts with the Rac signaling pathway. *Developmental biology* **209**, 111-127 (1999).

[4] Gally, C. et al. Myosin II regulation during C. elegans embryonic elongation: LET-502/ROCK, MRCK-1 and PAK-1, three kinases with different roles. *Development* (Cambridge, England) **136**, 3109-3119 (2009).

[5] Chan, B.G., Rocheleau, S.K., Smit, R.B. & Mains, P.E. The Rho guanine exchange factor RHGF-2 acts through the Rho-binding kinase LET-502 to mediate embryonic elongation in C. elegans. *Developmental biology* (2015).

[6] Diogon, M. et al. The RhoGAP RGA-2 and LET-502/ROCK achieve a balance of actomyosin-dependent forces in C. elegans epidermis to control morphogenesis. *Development* (Cambridge, England) **134**, 2469-2479 (2007).

[7] Shelton, C.A., Carter, J.C., Ellis, G.C. & Bowerman, B. The nonmuscle myosin regulatory light chain gene mlc-4 is required for cytokinesis, anterior-posterior polarity, and body morphology during Caenorhabditis elegans embryogenesis. *The Journal of cell biology* **146**, 439-451 (1999).

[8] Piekny, A.J., Johnson, J.L., Cham, G.D. & Mains, P.E. The Caenorhabditis elegans nonmuscle myosin genes nmy-1 and nmy-2 function as redundant components of the let-502/Rho-binding kinase and mel-11/myosin phosphatase pathway during embryonic morphogenesis. *Development* (Cambridge, England) **130**, 5695-5704 (2003).

[9] Liu, J., Maduzia, L.L., Shirayama, M. & Mello, C.C. NMY-2 maintains cellular asymmetry and cell boundaries, and promotes a SRC-dependent asymmetric cell division. *Developmental biology* **339**, 366-373 (2010).

[10] Costa, M. et al. A putative catenin-cadherin system mediates morphogenesis of the Caenorhabditis elegans embryo. *The Journal of cell biology* **141**, 297-308 (1998).

[11] Lockwood, C., Zaidel-Bar, R. & Hardin, J. The C. elegans zonula occludens ortholog cooperates with the cadherin complex to recruit actin during morphogenesis. *Current biology : CB* **18**, 1333-1337 (2008).

[12] Simske, J.S. et al. The cell junction protein VAB-9 regulates adhesion and epidermal morphology in C. elegans. *Nature cell biology* **5**, 619-625 (2003).

[13] Kasza, K.E. et al. The cell as a material. *Curr. Opin. Cell Biol.* **19**, 101-107 (2007).

[14] Theocaris, P.S., Pazis, D. & Konstantellos, B.D. The Exact Shape of a Deformed Internal Slant Crack under Biaxial Loading. *Int J Fracture* **30**, 135-153 (1986).

[15] Rauzi, M. & Lenne, P.F. Probing cell mechanics with subcellular laser dissection of actomyosin networks in the early developing Drosophila embryo. *Methods in molecular biology* (Clifton, N.J.) **1189**, 209-218 (2015).

[16] Smutny, M., Behrndt, M., Campinho, P., Ruprecht, V. & Heisenberg, C.P. UV laser ablation to measure cell and tissue-generated forces in the zebrafish embryo in vivo and ex vivo. *Methods in molecular biology* (Clifton, N.J.) **1189**, 219-235 (2015).

[17] Mayer, M., Depken, M., Bois, J.S., Julicher, F. & Grill, S.W. Anisotropies in cortical tension reveal the physical basis of polarizing cortical flows. *Nature* **467**, 617-621 (2010).

[18] Bert, C.W. Models for Fibrous Composites with Different Properties in Tension and Compression. *J Eng Mater-T Asme* **99**, 344-349 (1977).

[19] Jones, R.M. Stress-Strain Relations for Materials with Different Moduli in Tension and Compression. *Aiaa J* **15**, 16-23 (1977).

[20] Murrell, M.P. & Gardel, M.L. F-actin buckling coordinates contractility and severing in a biomimetic actomyosin cortex. *Proceedings of the National Academy of Sciences of the United States of America* **109**, 20820-20825 (2012).

[21] Landau, L.D. & Lifshitz, E.M. Theory of Elasticity,*(Volume 7 of A Course of Theoretical Physics)*, Pergamon Press (1970).

[22] Freund, L.B. Dynamic Fracture Mechanics, *Cambridge Monographs on Mechanics*(1990).

[23] Muskkhelishvili, N.I Some basic Problems of the Mathematical Theory of Elasticity. *Noordhoff International Publishing*, Leyden (1975).

[24] Suo, Z. Singularirities, interfaces and cracks. *Proc. R. Soc. London, Ser. A* **427**, 331-358 (1990).

[25] Yoffe, E.H. The moving Griffith crack. *Philo. Mag.***42**, 739-50(1951).

[26] Lekhnitskii, S.G. Theory of elasticity of an anisotropic body, San Francisco: Holden day(1963).

[27] Wu ,M. & Ben Amar, M. Modelling fibers in growing discs of soft tissues. *Journ. Math. And Mech. of solids* **39** (2): 219-224 (2014)

[28] Ben Amar, M. Wu, M. Trejo, M. & Atlan, M. Morpho-elasticity of inflammatory fibrosis: the case of capsular contracture. *Journ. Roy. Soc. Interface* **12** 20150343 (2015)

[29] Ogden, R.W. Non-linear elastic deformations, *Dover Publications and Ellis Horwood* (1984)

[30] Gasser , T.R. Ogden, R.W. & G. Holzapfel, G. Hyperelastic modelling of arterial layers with distributed collagen fiber orientation. *J.R.Soc. Interface* **3**,15-35(2006).

[31] Destrade, M. Incremental equations for soft fibrous materials, Nonlinear Mechanics of Soft Fibrous Materials .*CISM Lecture Notes*, R.W. Ogden & L. Dorfmann, Editors, Springer, **559** 233-267 (2015)